Nano Energy 70 (2020) 104436

Contents lists available at ScienceDirect

Nano Energy

journal homepage: http://www.elsevier.com/locate/nanoen

Full paper

A flexible, ultra-highly sensitive and stable capacitive pressure sensor with convex microarrays for motion and health monitoring

Yaoxu Xiong [a,b], Youkang Shen [a,c], Lan Tian [a], Yougen Hu [a,*], Pengli Zhu [a,**], Rong Sun [a], Ching-Ping Wong [d]

[a] Shenzhen Institute of Advanced Electronic Materials, Shenzhen Institutes of Advanced Technology, Chinese Academy of Sciences, Shenzhen, 518055, PR China
[b] Shenzhen College of Advanced Technology, University of Chinese Academy of Sciences, Shenzhen, 518055, PR China
[c] College of Materials Science and Engineering, Shenzhen University, Shenzhen, 518055, PR China
[d] School of Materials Science and Engineering, Georgia Institute of Technology, Atlanta, GA, 30332, USA

ARTICLE INFO

Keywords:
Flexible capacitive pressure sensor
Sensitivity
Dielectric layer
Self-assembly
Motion monitoring
Finite element analysis (FEA)

ABSTRACT

Recently, flexible sensors endowed with high sensitivity, low detection limit, broad working pressure range and fast response have aroused widespread concern owing to their vital role in the development of wearable artificial devices, human-machine interaction and healthcare systems. Herein, flexible and highly sensitive capacitive pressure sensors were fabricated based on flexible electrodes with convex microarrays and ultrathin dielectric layer. The proposed sensor is constructed by sandwiching a top micro-arrayed electrode, a middle ultrathin dielectric layer and a bottom micro-arrayed electrode, and it demonstrates an ultra-high sensitivity of 30.2 kPa^{-1} (0–130 Pa), fast response time of 25 ms, low detection limit of 0.7 Pa and extreme stability of 100 000 cycles without fatigue. The finite-element analysis indicates that the changes of contact area and distance between two electrodes under external stimulus are critical to achieve superior properties of the sensor. Benefitting from the outstanding comprehensive performance, the enormous potential ability of the capacitive sensor in monitoring physiological signals and robot hand grabbing motions have been successfully demonstrated, which indicates promising applications in wearable intelligent electronic devices.

1. Introduction

With the growing demands for booming artificial intelligence and the internet of thing (IoT), flexible pressure sensor as one of the crucial sensing elements has been attracted great attention due to their promising applications in wearable electronic devices for medical diagnosis [1–5], healthcare monitors [6–15], human-machine interaction [16] and smart home [17,18], *etc*. To distinguish external stimulus, flexible pressure sensors usually convert the applied force into recognizable electrical signals or other responsive output signal. To some extent, the flexible sensors can help the inanimate objects to understand how human "feel" during interactions, as well as obtain biological signals such as blood pressure and body motions. The key parameters including sensitivity, response time, limit of detection (LOD) and working stability were generally used to evaluate the performance of pressure sensors. According to the sensing mechanism, there were four typical types including piezoresistive [6,8,9,19–21], capacitive [22–27], piezoelectric [28–32], and triboelectric [33–37] sensors. Among them, the flexible capacitive pressure sensors (FCPS), which can be integrated into the irregular surfaces such as touch screen, flexible display and even human skin, were widely researched owing to their advantages of high sensitivity, fast response and low hysteresis.

Similar to the traditional plane-parallel capacitor, the FCPS generally consists of two thin parallel flexible conducting flats (top electrode and bottom electrode) separated by a dielectric layer typically of polyvinylidene fluoride (PVDF) and methacrylate, etc. The flexible electrodes were mainly fabricated by coating conductive materials on the surface of flexible substrates (polydimethylsiloxane (PDMS), polyethylene terephthalate (PET), polyimide (PI), polyvinyl alcohol (PVA), *etc.*) or adding conductive fillers (metal micro-flakes, silver nanowires, graphene, carbon nanotubes, *etc.*) into polymer matrix. The capacitance (C) of a parallel plate capacitor is generally defined as the ratio of the charge carried by a capacitor to the voltage between electrodes and determined by the distance between two electrodes (d), the effective

* Corresponding author.
** Corresponding author.
E-mail addresses: yg.hu@siat.ac.cn (Y. Hu), pl.zhu@siat.ac.cn (P. Zhu).

https://doi.org/10.1016/j.nanoen.2019.104436
Received 29 September 2019; Received in revised form 7 December 2019; Accepted 24 December 2019
Available online 9 January 2020

area of two electrodes (A) and the permittivity (ε) of dielectric layer, expressed as $C = \varepsilon A/4\pi kd$. For the FCPS with high sensitivity, both the electrodes and dielectric layer are required to be as flexible as possible so that the dielectric layer and electrodes can be deformed upon slight pressure stimulation, ultimately resulting in a remarkable change in capacitance.

In order to improve the sensitivity of FCPS, the different microstructures such as wave [12,26], pillar [1,38], pyramids [39–41], and micro-convex [11,42] were popularly introduced either as an electrodes or dielectric layer due to the easy deformation under external stimulus as compared with flat substrates and resulting into larger changes of d and A. For example, Park's group [43] used porous Ecoflex as a dielectric layer to fabricate sensor with sensitivity of 0.6 kPa^{-1}, while without pores was 0.016 kPa^{-1}. Guo's group [44] used rose petals and leaves with microstructure as dielectric layers of the sensor to obtain a high sensitivity of 1.54 kPa^{-1}. Gui's [22] group applied low-cost nylon netting as dielectric layer to improve sensitivity (0.33 kPa^{-1}). Zhu's group [12] prepared wavy microstructure by pre-stretching method to improve sensor sensitivity (2.94 kPa^{-1}). Zhang's group [24] transferred the microstructure of the lotus leaf to the surface of PMDS by two-step replication as electrodes and used polystyrene microspheres as the dielectric layer to prepare flexible pressure sensor with a high sensitivity of 0.815 kPa^{-1}, while without lotus leaf' microstructure was only 0.038 kPa^{-1}. However, the sensitivities of these sensors are still relatively low to obtain distinct and stable signals along with high signal to noise ratio (SNR). Therefore, the FCPS with ultra-high sensitivity and excellent working stability are still highly desirable.

Herein, we developed an ultra-highly sensitive capacitive sensor integrated by two PDMS-Au electrodes with surface convex microarrays and an ultrathin PVDF dielectric layer using a simple and low-cost strategy. The convex microarrays were fabricated via a colloidal self-assembly and two-step replication process, and the PVDF film was prepared by a facile spin-coating method. The proposed flexible capacitive pressure sensor exhibits an ultrahigh sensitivity of 30.2 kPa^{-1} in pressure regime of <130 Pa, low detection limit (0.7 Pa), extremely high stability (100 000 cycles) under 15 Pa with loading/unloading frequency of 1 Hz. Based on the superior performance, the applications of the capacitive sensor in monitoring various human biological signals of respiration, pronunciation and body motions, and also robot hand grabbing motions were further visually demonstrated with excellent stability and high signal-to-noise ratio. Moreover, the finite-element analysis was applied to analysis the changes of contact area and distance between two electrodes, the results illustrated that the microarrays on the surface of electrode and ultrathin dielectric layer were synergistically caused significant increase in high sensitivity.

2. Experimental section

2.1. Materials

Uniform sized polystyrene (PS) microspheres (0.5, 2, 5.6 μm of diameter) were synthesized via a modified dispersion polymerization method as described in our previous report [45]. PDMS prepolymer (Sylgard 184) and curing agent were acquired from Dow Corning, polyvinylidene fluoride (PVDF) powder was obtained from Sigma-Aldrich with the molecular weight of 200000. Sulfuric acid (H_2SO_4, 98%), N-methyl pyrrolidone (NMP, AR), hydrogen peroxide (H_2O_2, 30%) and ethanol (C_2H_5OH, 98%) were supplied by Sinopharm Chemical Reagent Co. Ltd. (Shanghai, China). Ultrapure water (>18 MΩ cm^{-1}) was used for all experiments.

2.2. Preparation of PS microspheres array by colloidal self-assemble method

Glass disks (diameter of 5 cm) were cleaned in piranha solution (a 3:7 mixture of H_2O_2 and H_2SO_4, volume ratio) at 80 °C to form hydrophilic surfaces, followed by repeated rinsing with deionized water, and then dried under a nitrogen flow. Please note that this mixture is extremely dangerous and should be carefully used in a fume hood. The PS microspheres (2 μm) were dispersed in ethanol/water (ethanol: water = 9:10, w/w) mixed solvent with concentration of 5 wt% via ultrasonication for 30 min. In the colloidal self-assemble process, 5 mL of deionized water was dropped to the cleaned glass surface to form a thin water layer and then PS suspension was dropwise added to the water edge. PS microspheres were self-assembled at the solid-liquid-gas (PS-water/ethanol-air) three-phase interface and formed a uniform PS array after water and ethanol were completely evaporated at room temperature. The self-assembly process of 0.5 and 5.6 μm PS microspheres array was the same as 2 μm microspheres array.

2.3. Preparation of PDMS electrode with surface convex microarrays

The flexible PDMS electrode with surface convex microarrays were fabricated via a two-step replication process. Firstly, liquid PDMS (prepolymer: curing agent = 10: 1, w/w) was spin-coated on the glass with surface self-assembled 2 μm PS microspheres at 200 rpm for 10 s, followed by heat curing at 100 °C for 2 h. The cured PDMS film was carefully separated from the glass and immersed in toluene solution for 30 min to fully remove the embedded PS microspheres, leaving concave microarrays on the PDMS film surface. Then, the concave PDMS was treated by plasma (Femto, 50 mW, 1.0 bar) for 10 min. Followed by spinning coating another layer of liquid PDMS at 200 rpm for 10 s and cured at 80 °C for 2 h. After the above two-step replication process, the two cured PDMS layers were separated from each other to obtain the PDMS film with surface convex microarray. Finally, a conductive gold layer with thickness of about 100 nm was sputtered on the surface of the PDMS with micro-convex array, forming the flexible electrode with 2 μm convex microarrays. The preparation of flexible electrode with 0.5, 5.6 μm was the same with flexible electrode with 2 μm.

2.4. Preparation of dielectric film

The PVDF/NMP solution (PVDF: NMP = 1:10, w/w) was formulated by dissolving a desired amount of PVDF powder in NMP solvent, and then uniformly spin-coated on a cleaned glass substrate at 600 rpm for 10 s. After dried at 80 °C for 30 min, the PVDF film (4 μm) was slowly peeled off from the glass. The different thickness of dielectric layer about 7 μm and 10 μm were obtained at 400 rpm and 200 rpm for 10 s, respectively. The process of preparation of PVA and PE dielectric layer is the same with that of PVDF dielectric layer.

2.5. Fabrication of the FCPS

In the process of fabrication of FCPS, the 2 μm micro-structured PDMS electrode was cut into strips, the silver leads were connected with external test equipment using commercial conductive silver paste at one end of the cut electrode with surface gold layer. Next, two PDMS electrodes and a different thickness dielectric film were sandwiched into a flexible pressure sensor with the PVDF film as a middle layer. The sensor with 0.5, 5.6 μm micro-structured PDMS electrode was prepared in the same way as the sensor with 2 μm micro-structured PDMS electrode.

2.6. Characterization

The morphologies of the PDMS films with concave microarrays and the PVDF films were characterized by a field emission scanning electron microscope (FE-SEM, FEI Nano SEM 450). The Young's modulus and dielectric constant of dielectric materials were measured by an electronic universal testing machine (Suns, UTM2102) and precision impedance analyzer (Agilent 4294A), respectively. The capacitance was measured by LCR digital bridge tester (Gwinstek, LCR-6002). The

sensitivity and cyclic stability of the FCPS were tested via electronic universal testing machine (Shimadzu AG-X plus, 100 N). A robot hand (i-LIMB hand, Tough Bionics) was used to grab objects.

2.7. Finite element analysis method

To calculate the contact area and distance between two electrodes under external pressure, structural analysis was conducted via finite element simulation. The sizes of sandwich structure applied in finite element simulated are consistent with that actual measurement values. In detail, the microarrays are closely packed with a convex size of 2 μm. In order to obtain accurate simulation results, the cells were messed according to different contact surfaces (element size: 0.2 (minimum) and 1.0 (maximum)), and the messed mode is based on triangle. The growth step is 0.1, and a total of 50 steps are calculated. The contact model is based on the surface-to-surface contact among the deformable sandwich structures.

3. Result and discussion

The fabrication approach of making flexible pressure sensor with uniform microstructure array was schematically illustrated in Fig. 1. The adopted simple fabrication steps, low cost, and self-assembling process could be interesting in future reliable pressure sensor fabrication. Fig. 1a–g illustrated the process of fabricating electrode with concave microstructure and Fig. 1h–k demonstrated how to prepare dielectric layer. Finally, it revealed the sandwich structure of flexible pressure sensor via layer by layer method as shown in Fig. 1*l*. The whole fabrication process details were described in the Experimental Section. Fig. 1m showed the whole structure of the sensor, the sandwiched sensor was fixed by the package layer A and package layer B. Fig. 1n visually demonstrated the flexibility of the packaged sensor, which could be bended to a little circle with diameter of 7 mm and attached to the arm.

Fig. 2a shows the SEM image of the self-assembled 2 μm polystyrene microspheres array. It demonstrates uniform PS spheres were regularly and closely packed on the glass substrate forming a monolayer array. Fig. 2b shows the SEM image of the first PDMS film fabricated by spin coating liquid PDMS on PS array surface and remove PS array after heat curing. It clearly reveals that there are a number of uniform concavities on the surface of PDMS, and the diameter of the concavity is ~2 μm, which is consistent with the size of PS microspheres. These concavities were remained from the PS spheres array embedded in PDMS film surface and completely sacrificed after immersing in toluene. As demonstrated in Fig. 2c, the PDMS film with convex array was obtained after the second replication process. It can be seen that the micro-structured PDMS with diameter of ~2 μm is regularly and closely arranged. At the same time, due to the uniform microstructure on the surface of PDMS, PDMS film forms brilliant colors through the refraction,

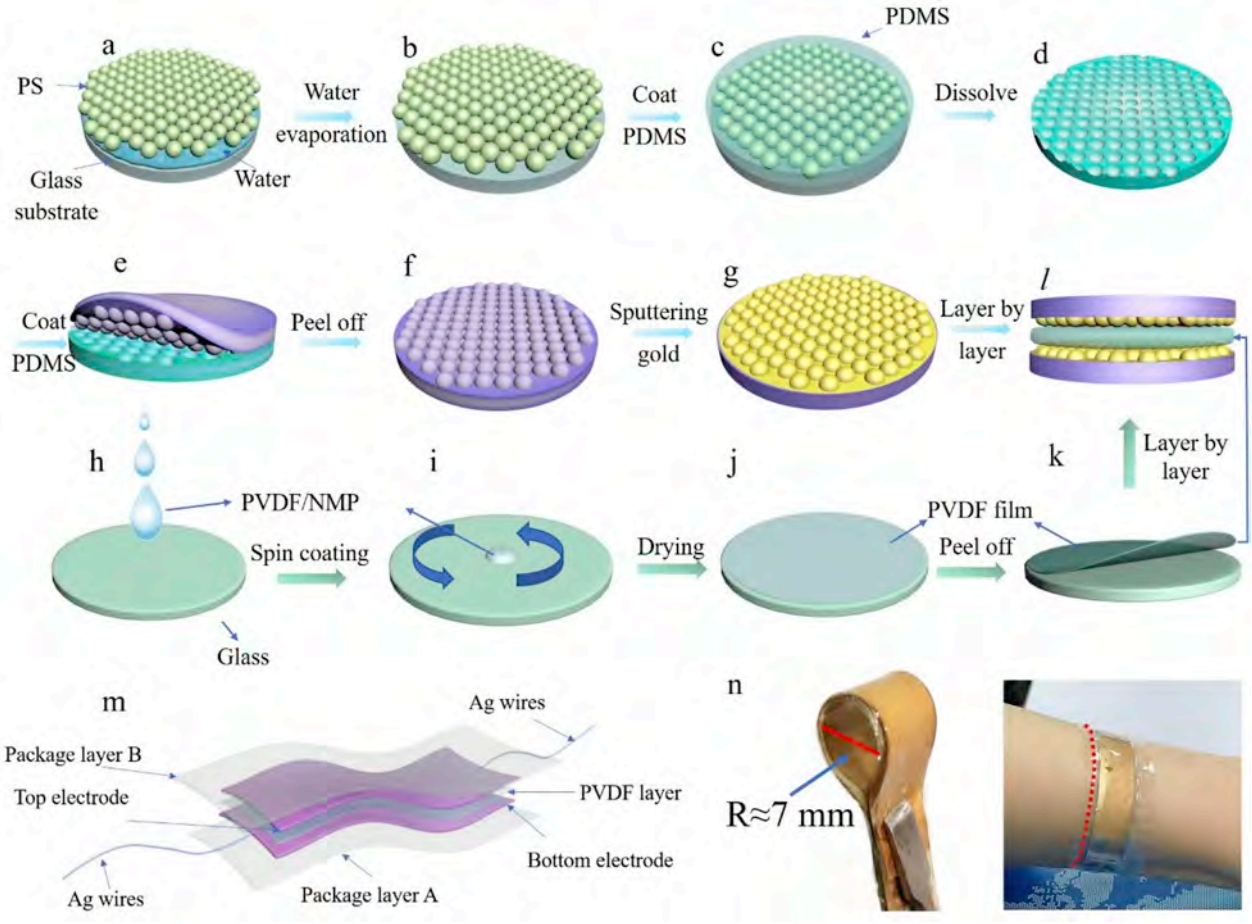

Fig. 1. Schematic diagram of the fabrication process of the flexible capacitive pressure sensor with microarrays. a) Self-assembly of polystyrene (PS) spheres at the solvent/air interface. b) Monolayer PS spheres array on the surface of glass after solvent evaporation. c) Spin coating and heat curing the first PDMS layer on the surface of PS spheres array. d) PDMS film with surface concave microstructure after dissolving PS spheres. e) Spin coating and heat curing the second PDMS layer on the first cured PDMS film. f) The second cured PDMS with surface convex microstructure. g) Sputtering Au layer on the surface of the PDMS film with convex microstructure. h-k) Fabrication of PVDF film by spin coating of PVDF/NMP solution on a glass substrate followed by heating dry. l) Integration of the pressure sensor by sequentially sandwiching a top PDMS-Au electrode, a middle PVDF dielectric layer and a bottom PDMS-Au electrode face to face. m) The integrated structure of the packaged sensor. and n) Flexibility demonstration of the packaged sensor.

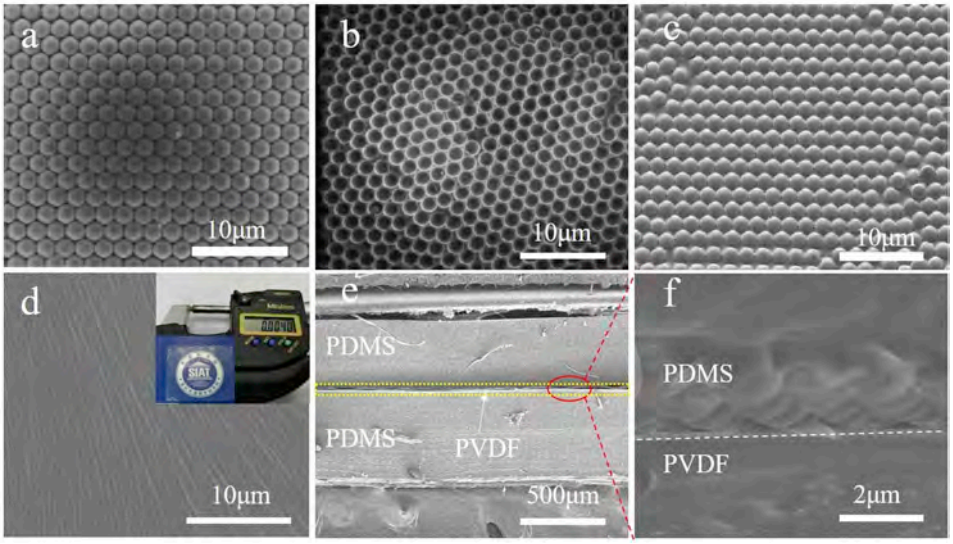

Fig. 2. a) SEM image of the self-assembled PS microspheres array. b) SEM image of PDMS film with surface concave microstructure. c) SEM image of PDMS film with surface convex microstructure. d) SEM image and thickness measurement of the PVDF film. e) The cross-sectional SEM image of the sandwiched flexible pressure sensor. and f) Partial enlarged image of (e).

diffraction and interference of light (Fig. S1 in the Supporting Information). The SEM images of the convex PDMS film with 0.5 and 5.6 μm microarrays were shown in Fig. S2. The results proved that PDMS film with surface convex array can be successfully fabricated by a simple two-step replication process with assistance of a colloidal self-assembly method. Fig. 2d shows the SEM image of PVDF film fabricated by spin coating method and the thickness is 4 μm tested by a spiral micrometer. The cross-sectional SEM image of the sandwiched flexible pressure sensor was shown in Fig. 2e. It can be seen that the top and bottom PDMS electrodes are separated by an ultra-thin dielectric layer of PVDF film. Fig. 2f is a partial enlarged SEM image of Fig. 2e, which shows the detailed feature of the interface area of the micro-structured PDMS electrode and the PVDF dielectric layer in close contact state.

In order to optimize the size of microarrays and dielectric materials to obtain the sensor with high sensitivity, the sensor with microarrays of 0.5, 2 and 5.6 μm and dielectric materials of PVDF, PVA and PE was firstly investigated. The sensitivity of the above sensors was evaluated and the results are shown in the following Fig. S3. It can be seen that the sensitivity of sensors with convex microarrays is 5.7, 30.2 and 8.9 kPa^{-1} at pressure range of 0–220, 0–130 and 0–180 Pa for the microstructures of 0.5, 2 and 5.6 μm, respectively. The sensor using PVDF, PVA and PE as the dielectric layer shows different sensitivity, from high to low in order, as presented in Fig. S4. Based on these results, microarrays with 2 μm and PVDF dielectric layer was selected to construct the FCPS for high sensitivity.

To evaluate sensor performance on the effect of interface between the dielectric layer and microarray convex structure, the FCPS were fabricated with different thickness of the PVDF layers such as 4, 7 and 10 μm named as FCPS-MD4, FCPS-MD7, and FCPS-MD10, respectively. For comparison, the FCPS-FD4 was abridged with flat PDMS (500 μm) and 4 μm PVDF under similar experimental conditions. The flexible capacitive pressure sensor with flat electrodes and 4 dielectric layers were abridged as FCPS-FD4. Based on the formula of $S = \delta(\Delta C/C_0)/\delta P$, the sensitivity of the flexible pressure sensor can be calculated by depicting the slope of the tangent line on pressure-capacitance rate curve. To discuss the influence of the convex microarray and the ultra-thin dielectric layer to the performance of FCPS, a consecutive pressure from 0 to 10 kPa was loaded on the FCPS-MD4, FCPS-MD7, and FCPS-MD10, respectively. And the FCPS-FD4 was used as a blank control group. As demonstrated in Fig. 3a, two linear regions where the change rate of capacitance as a function of pressure were observed. In the low pressure rang (0–130 Pa), the sensitivity of FCPS-MD4 was up to 30.2 kPa^{-1}, much higher than most of the previous reports as exhibited in Table S1 (Supporting Information). In the high pressure rang (130 Pa-10 kPa), the FCPS-MD4 demonstrated a sensitivity of 0.47 kPa^{-1}. The linear relationship in the range of 0–130 Pa was zoomed up in Fig. S5. It clearly reveals that there is an excellent linear relationship in the pressure range of 0–130 Pa with a high correlation coefficient of 0.97. This ultrahigh sensitivity was mainly attributed to the convex microarrays and ultra-thin dielectric layer. For the FCPS-FD4, the capacitance curve (black dotted line) presents a linear trend with low sensitivity of 0.89 kPa^{-1} (0–1.8 kPa) and 0.39 kPa^{-1} (3–9 kPa). It proved that the existence of the convex microarrays on the electrodes surface can obviously improve the sensitivity of the sensor because of the various contact area under different pressure.

To investigate the effect of the thickness of PVDF dielectric layer on the sensitivity of the FCPS, the capacitance-pressure curves were measured of the sensors with different dielectric layer thicknesses of 4, 7 and 10 μm. The results show that FCPS-MD4 was much higher than that of the FCPS-MD7 (24 kPa^{-1}, 0–200Pa; 0.25 kPa^{-1}, 4–9 kPa) and FCPS-MD10 (4.3 kPa^{-1}, 0–200 Pa; 0.53 kPa^{-1}, 4–9 kPa). The zoomed up and linear fitting curves in Fig. 3a were presented in Fig. S6 in the Supporting Information for more clear observation. It can be explained that the thickness changes of the PVDF dielectric layer with different thicknesses are the same under the same pressure conditions, however, considering their different initial thicknesses, the relative change rate of the inter-planar spacing was different. As shown in Fig. 3a, when the thickness of the dielectric layer reduces from 10 to 7 and 4 μm, the sensitivity of the sensor gradually increases, indicating that the sensitivity of the sensor is inverse correlation to the thickness of the dielectric layer. The change in the contact area and the parallel plate distance under external pressure will synergistically improve the sensitivity of the sensor. It should be noted that, when the thickness of the dielectric layer is too thin especially close to the size of microarrays, it will be easily damaged and resulting into failure of the sensor upon external loading stimulation due to modulus mismatch and stress concentration at the contact points between the dielectric layer and the microarrays. The smaller of the inter-planar spacing, the greater the rate of change of the inter-planar spacing, especially occured when the thickness of the dielectric layer was close to the height of the microarrays. The synergistic effect of the changed contact area and the changed inter-planar spacing causes a sharp change in the capacitance value, thereby improving the sensitivity

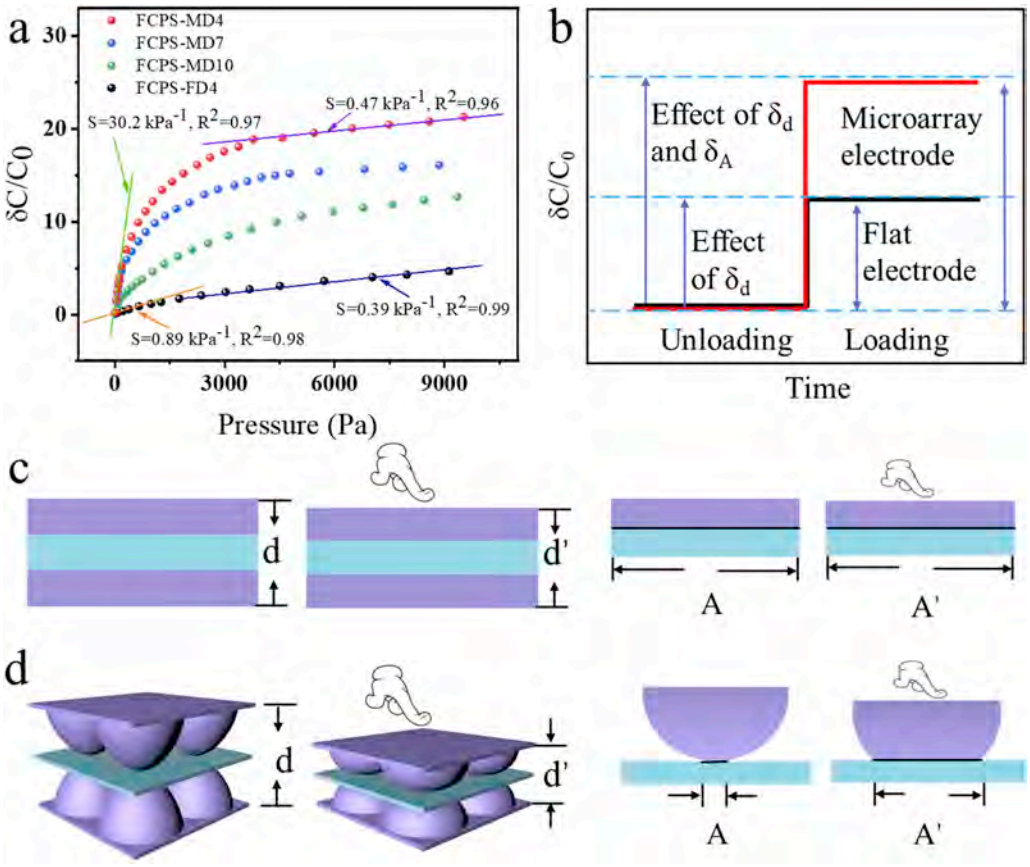

Fig. 3. a) Sensitivity comparison of different flexible sensors. b) Effect of dielectric layer thickness and contact area on the sensitivity. c) Schematic diagram of distance and contact area changes when FCPS-FD was loaded. d) Schematic diagram of distance and contact area changes when FCPS-MD was loaded.

of the sensor.

Fig. 3b provides schematic illustration for the rate of capacitance change under the external pressure where the "δ_d" and "δ_A" are represented the changes of parallel plate height and contact area, respectively. For the pressure loading on the FCPS-FD4, δ_A is almost constant which has negligible effect on the change of capacitance. δ_d caused by the deformation of elastomeric dielectric layer contributes to the various capacitance. For the pressure loading on the FCPS-MD4, the δ_d and δ_A jointly dedicate to the changes in capacitance. More details are illustrated in Fig. 3c and d. When external pressure was loaded on the FCPS-FD4, the contact area was hardly changed and the deformation of dielectric layer thickness was the main factor resulting in various of relative capacitances. However, the FCPS-MD4 was easier to be deformed under the same pressure as compared with FCPS-FD4 because external pressure was focused on microstructure rather than the whole flat, resulting patented microarrays were easier to be deformed which reflected in δ_d and δ_A. So, for the FCPS-MD4, not only the distance between two electrodes but also the contact area was dramatically changed under applied pressure, leading to observable improvement of its sensitivity.

The sensing mechanism was further validated from finite element analysis (FEA) and the results were shown in Fig. 4. The schematic diagram (Fig. 4a) shows model flexible capacitive pressure sensor integrated by two gold coated PDMS films with surface convex microarrays. A dielectric layer PVDF sandwiched between the gold coated microarrays and two silver leads were attached to the top and bottom gold coated PDMS electrodes. Fig. 4b exhibits the deformations of the convex microarrays under external pressure. The deformations will increase the contact area as well as decrease the distance between two electrodes, consequently generating remarkable capacitance signals.

In order to investigate how the microarrays and the thickness of dielectric layer affect the sensing performance of the as-prepared capacitive sensor, FEA was applied in simulating the deformation against with external pressure. A similar sensor integrated by two PDMS films without microarrays was used as control. Fig. 4c–f shows the sensor was deformed under pressures of 10, 20, 30, and 40 kPa, respectively. As demonstrated in Fig. 4c, for the control sensor without microarrays, the whole contact surface was deformed under external force and the stress was uniformly distributed due to the contact surface is flat and continuous, resulting in a low change rate of the relative inter-planar spacing. In this case, the change value of the capacitance is dominantly affected by the decrease of the distance between two electrodes because the contact area is hardly changed. So, there is a low capacitance change rate due to the small change of the inter-planar spacing, ultimately resulting in a low sensitivity. However, for the flexible sensors with microarrays (Fig. 4d–f), due to there are a number of discontinuous convex microarrays, the mechanical deformation of the flexible electrodes as the function of pressure will gradually increase the contact area as well as decrease the distance between two flexible electrodes, eventually improving the sensitivity of the sensor. Compared to the unstructured flexible electrode, the force on discontinuous microstructure is more concentrated on microarrays under the same pressure conditions, generating larger deformation. So, the ratios of δd/d (changed in height) and the contact area δA/A (changed in horizontal) are higher than that of the flat PDMS electrode (Movie S4, Supporting Information).

Supplementary data related to this article can be found at https://doi.org/10.1016/j.nanoen.2019.104436.

In the FEA press-mode operation, the concrete data in FEA of contact area and distance are depicted in Fig. 4g–j. It can be seen from Fig. 4g that the change rate of the contact area of the flexible electrode without the microarrays is almost a horizontal line, which means that the contact

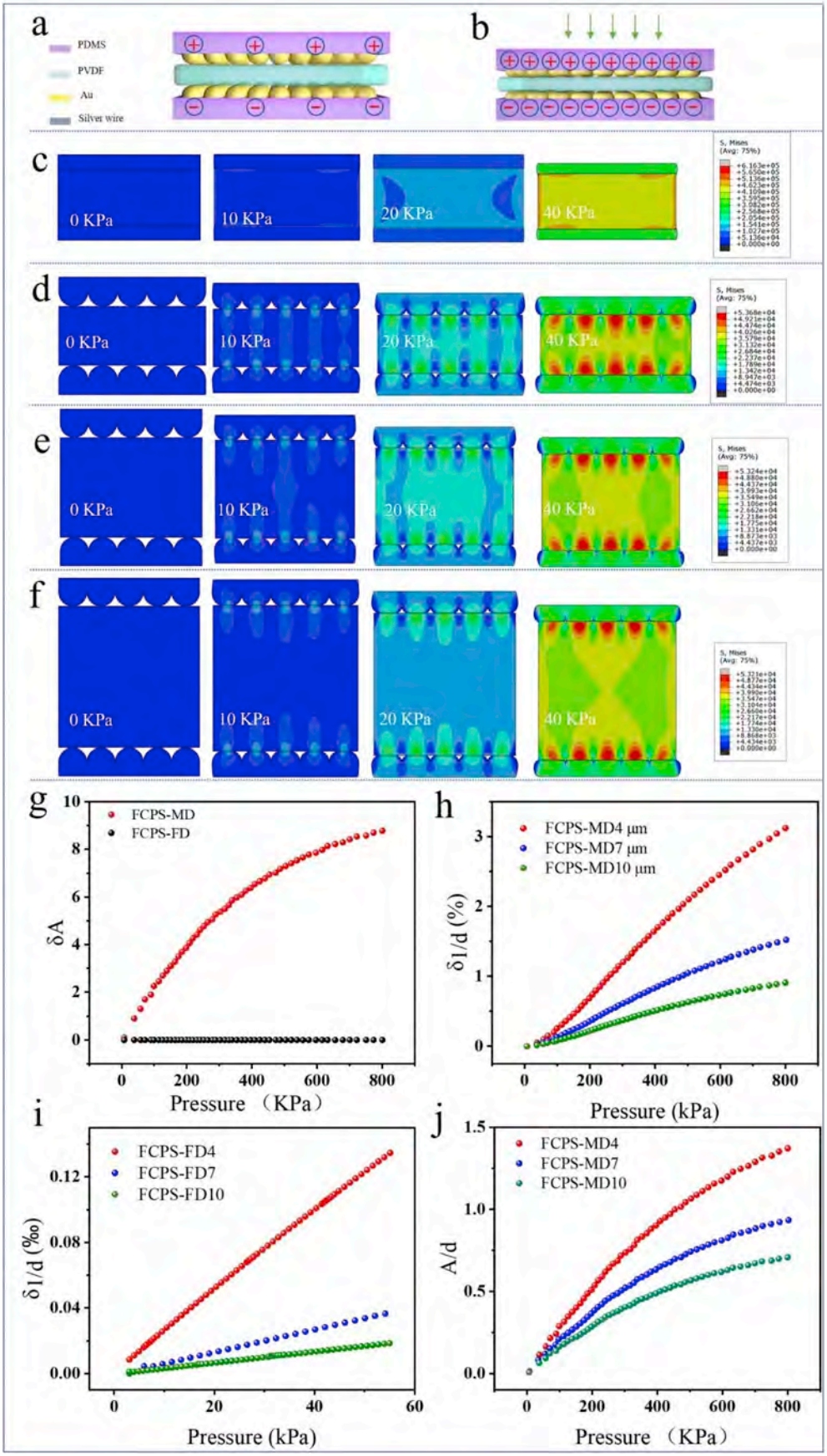

Fig. 4. Simulation results of the flexible capacitive pressure sensors. a) Diagram of the capacitive sensor composition. b) Schematic diagram of the contact area of the sensor under external pressure. c) Force analysis cloud diagram of the FCPS-FD4. d) Force analysis cloud diagram of the FCPS-MD4. e) Force analysis cloud diagram of the FCPS-MD7. f) Force analysis cloud diagram of the FCPS-MD10. Fig. 4 g) FEA simulates the results of changed contact area. h) FEA simulates the results of distance between two microstructured electrodes. i) FEA simulates the results of distance between two flat electrodes. j) FEA simulates the results of A/d of microarrayed sensor.

area of the continuous flat structure is hardly changed under the pressure action. However, the change rate of the contact area of the flexible electrode with microarrays increases rapidly with the increase of the pressure, and the change rate of the contact area increases slowly when the pressure exceeds a certain range. Moreover, it can be seen from Fig. 4h that the reciprocal change of distance for FCPS-MD4 is higher than that of FCPS-MD7 and FCPS-MD10, revealing sensitivity curve is inversely proportional to the dielectric layer thickness, which is agreed with previous experiment results. Similarly, for the sensor with flat electrode, Fig. 4i shows that the change rate of *d* is inversely proportional to the dielectric layer thickness. Based on the results of Fig. 4g–i, the quantitative relationship between A/d and applied pressure was obtained as shown in Fig. 4j (micro-arrayed electrodes) and Fig. S7 (flat electrodes).

As definition of the capacitance and sensitivity as following equations:

$$S = \frac{\delta(C - C_0)/C_0}{\delta P}$$

the sensitivity can be further written to

$$S = \frac{\delta\left(\frac{C}{C_0} - 1\right)}{\delta P} = \frac{\delta\left(\frac{\frac{\varepsilon A}{4\pi k d}}{\frac{\varepsilon A_0}{4\pi k d_0}} - 1\right)}{\delta P} = \frac{\delta\left(\frac{d_0}{A_0} \times \frac{A}{d} - 1\right)}{\delta P}$$

where d_0 and A_0 is the initial distance and initial contact area of the sensor, respectively, and they are constants for every sensor. Therefore, for the curve of δ(A/d)-P, the sensitivity of the sensor can be calculated by its slope. From the results of the above simulations, we can draw three conclusions. The first, limited by the deformation ability of the microarrays, the sensitivity decreases slowly with the increase of pressure. The second, convex microarrays make great progress in improving sensitivity compared with flat film without microstructure. The third, the smaller thickness of the dielectric layer, the higher sensitivity of the sensor.

Response time and detection limit are also the significant parameters for FCPS-MD4, which were measured by applying lightweight objects as external pressure. In order to obtain a stable capacitance response signal in the process of loading and unloading cycles, a mica sheet was placed on the sensor to just cover the surface of sensor. Fig. 5a demonstrates the time-response curve of loading and unloading pressure with an exquisite handicraft on the FCPS-MD4. The acquired capacitance signal exhibits a

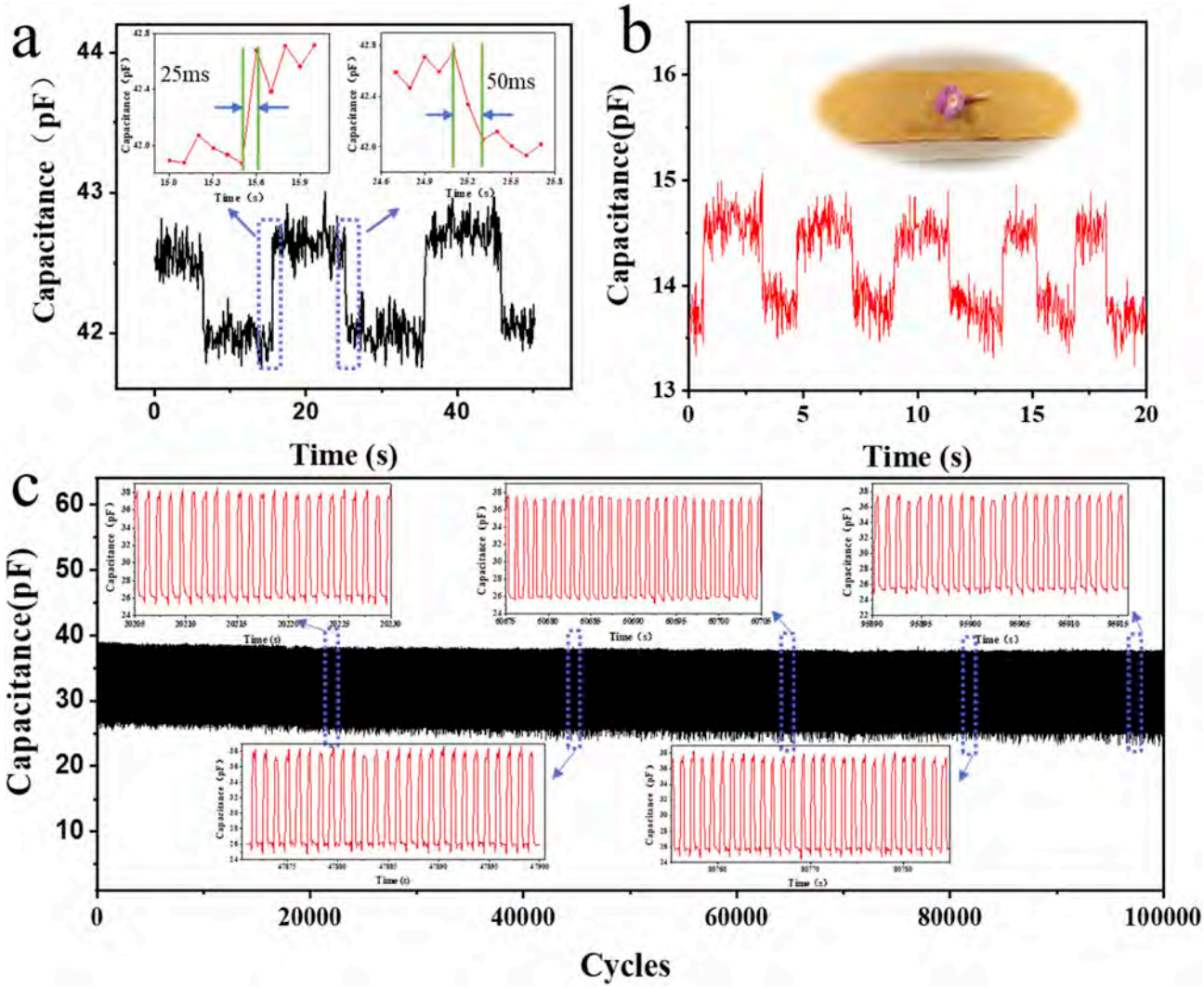

Fig. 5. a) Response time of the FCPS-MD4, the enlarged drawings show the blue part of the curve which corresponds to the loading/unloading of pressure. b) Corresponding capacitance signals of sever loading/unloading cycles for LOD test. c) Stability test (up to 100 000) of the FCPS-MD4 under the pressure of 15 Pa, the partially magnified pictures show the changed capacitance curves for different cycle stages.

short response time of 25 ms and 50 ms during the loading and unloading cycles, respectively. Fig. 5b shows a dried flower placed on the surface of FCPS-MD4 to apply a static pressure of 0.7 Pa. The static pressure is calculated through the equation of $P = mg/S$, where m is the dried flower mass of 8.2 mg, g is the gravity acceleration of 9.8 N/kg, and S is the valid area of the sensor of 0.9 cm × 1.3 cm. It can be clearly seen that the capacitance signal curve is regularly changed during the flower loading and unloading, indicating the sensor can distinctly detect tiny stimulus and translate into an obvious response signal. It can be clearly seen that the capacitance signal is regularly changed during the flower loading and unloading cycles, indicating that the sensor can distinctly detect tiny stimulus and translate into an obvious response signal. To further investigate the stability of the FCPS-MD4, external pressure (15 Pa) was dynamically loaded and unloaded onto the surface of the sensor with frequency of 1 Hz. As shown in Fig. 5c, the response performance was perfectly maintained even up to 100 000 loading/unloading cycles (Movie S1, Supporting Information), which reveals the outstanding repeatability and stability of the FCPS-MD4. The above results reveal that the as-prepared sensor has significant potential to detect subtle pressure with high accuracy and excellent long-term stability for practical application.

Supplementary data related to this article can be found at https://doi.org/10.1016/j.nanoen.2019.104436.

Physiological signals and body motions are important in human healthcare monitoring. Here, FCPS-MD4 was used to detect various motions such as breathe rating, pulse beating, pronouncing, elbow-bending, leg-bending and pressure distribution as shown in Fig. 6. The FCPS-MD4 sensor was attached to different body positions as given in

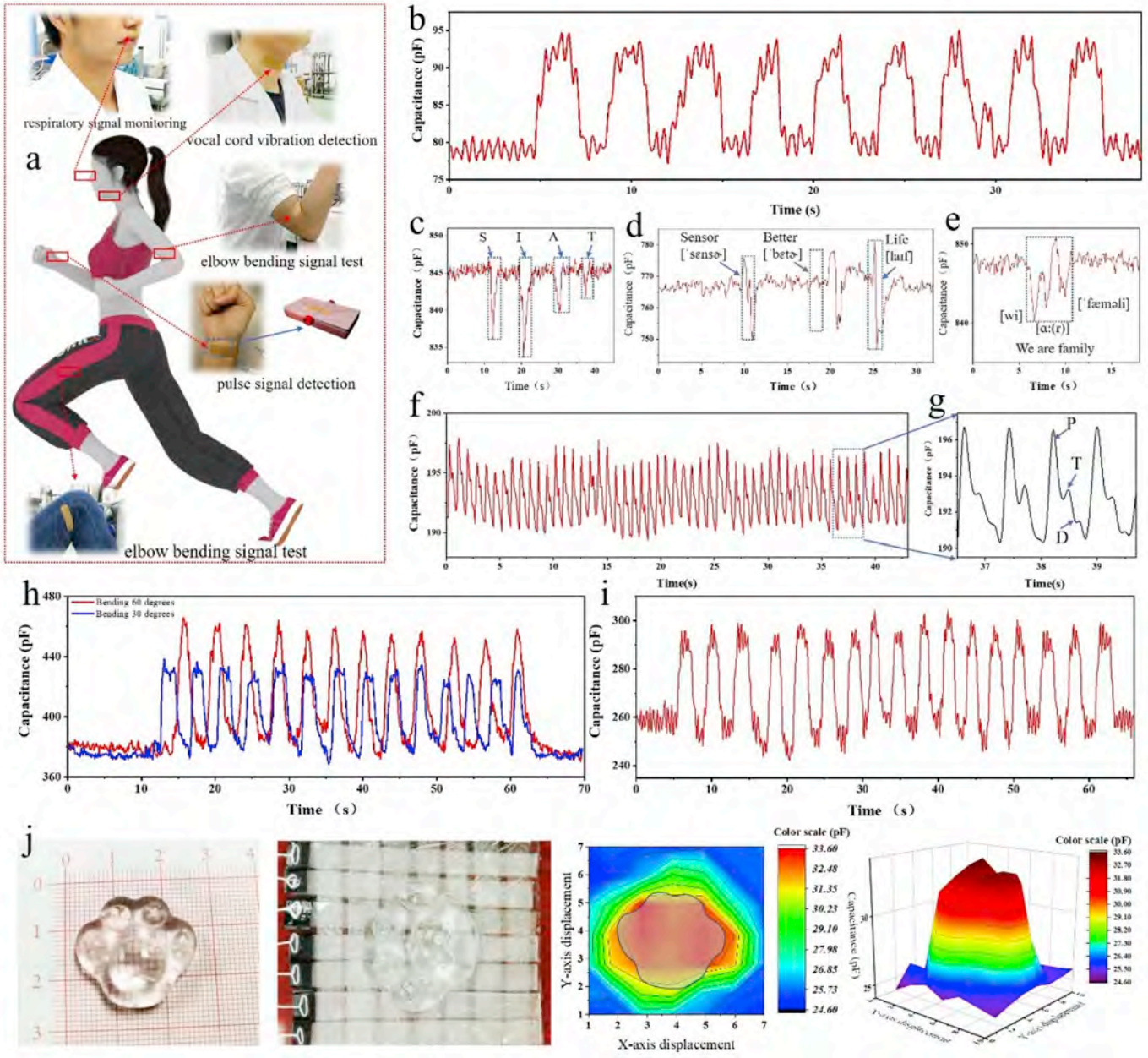

Fig. 6. Various applications of the FCPS-MD4. a) Schematic diagram of the FCPS-MD4 in detecting physical signals. b) Detection of the respiration rate by attaching the sensor on the philtrum. c) Detection of the vocal cord vibration signal caused by pronouncing multiple letters of "S", "I", "A" and "T". d) Detection of vocal cord vibration signal caused by multiple words of "sensor", "better" and "life". e) Detection of the vocal cord vibration signal caused by a sentence of "we are family". f-g) Detection of pulse signal in real time. h) Detection of elbow bending motions with bending angle of 60° and 30°. i) Detection of the leg bending motion. j) Cloud map of the pressure distribution detected by the capacitive sensor array.

Fig. 6a of philtrum, neck, wrist, arm and leg to detect various of human physiological signals of breath, voice, pulse beating, and elbow-bending, leg-bending, respectively. Detecting the respiration rate is significant for disorders, such as asthma and sleep apnea. Fig. 6b shows the breath signals acquired from the sensor to detect the pressure change caused by the airflow disturbance. The result reveals the breathing rate is 18 cycles/min when the volunteer in relaxation, demonstrating potential application of pressure sensor in medical monitoring abnormal respiration rates. Fig. 6c–e shows the acquired voice signals of pronunciation of letters, words and sentence, respectively, which caused by the movement of neck muscle and the vibration of vocal cord. Fig. 6c clearly shows the time-capacitance curve during pronunciation of the individual letters of "S", "I", "A" and "T". It can be seen that each letter's pronunciation including the weak consonant letter of "T" can be detected by the sensor and converted to capacitance peak. Fig. 6d and e also exhibit the characterized signal peaks of pronunciation of the words of "sensor", "better", "life" and even a sentence of "we are family", respectively. In order to illustrate the repeatability of the voice signal, detection of the repeated pronunciation was shown in Fig. S8. The fluctuation of the signal is related to the amplitude and frequency of the speaker voice during detection. The waveforms of five cyclic pronunciations of "We are family" exhibit excellent consistency and repeatability. These results reveal the flexible sensor can clearly distinguish vocal cord vibrations generated from pronunciation of no matter letters, words or sentence, illustrating promising potential of the sensor in analyzing of linguistic information. To demonstrate the application in pulse detecting (Movie S2, Supporting Information), the FCPS-MD4 was attached on the wrist of volunteer and the results are showed in Fig. 6f–g. The curve clearly shows the variation of capacitance caused by the pulse and it demonstrates stable and repeatable pulse shape including percussion wave (*P*-wave), tidal wave (*T*-wave) and dicrotic wave (*D*-wave), which are related with the systolic and diastolic blood pressure, ventricular rate, and heart rate respectively. Also, Fig. 6f reveals the resting heart rate of the volunteer was 76 beats per minute, which is the normal heart rate for adults. The sensor was also attached to the joint to detect the bending of the arm. As shown in Fig. 6h, when the arm was bent by ~30° and ~60°, the capacitance of the sensor is increased from 380 to 435 and 460 pF, respectively, and the sensor exhibited good signal resolution with continuous bending-relaxing cycles. Fig. 6i shows the leg bending signal by attaching the sensor to the thigh muscles. The uniform capacitive curve can be observed during running due to high sensitivity and excellent stability of the sensor. In order to illustrate the perception ability of spatial pressure distribution in a straightway, the FCPS-MD4 was assembled into a 7 × 7 array, and a transparent "bear's paw" mold was placed on the surface of the sensor array. As demonstrated in Fig. 6j, the red region (high pressure region) is basically consistent with the shape of the mold, which reveals the special pressure distribution of lightweight object (2.1763 g) can be clearly identified. These results illustrated the great potential of the flexible capacitive pressure sensor with convex microstructure as non-invasive medical devices for real-time monitoring of human health conditions.

Supplementary data related to this article can be found at https://doi.org/10.1016/j.nanoen.2019.104436.

To evaluate the sensing capabilities of the FCPS-MD4 used as a tactile sensor in actual applications, the capacitive sensor was attached to the surface of objects with different hardness, and the objects were grabbed by a robot hand as shown in Fig. 7a. The robot hand was manipulated by the robot control system, and the capacitance signal of the sensor was recorded in real time by a LCR tester and graphically displayed on the

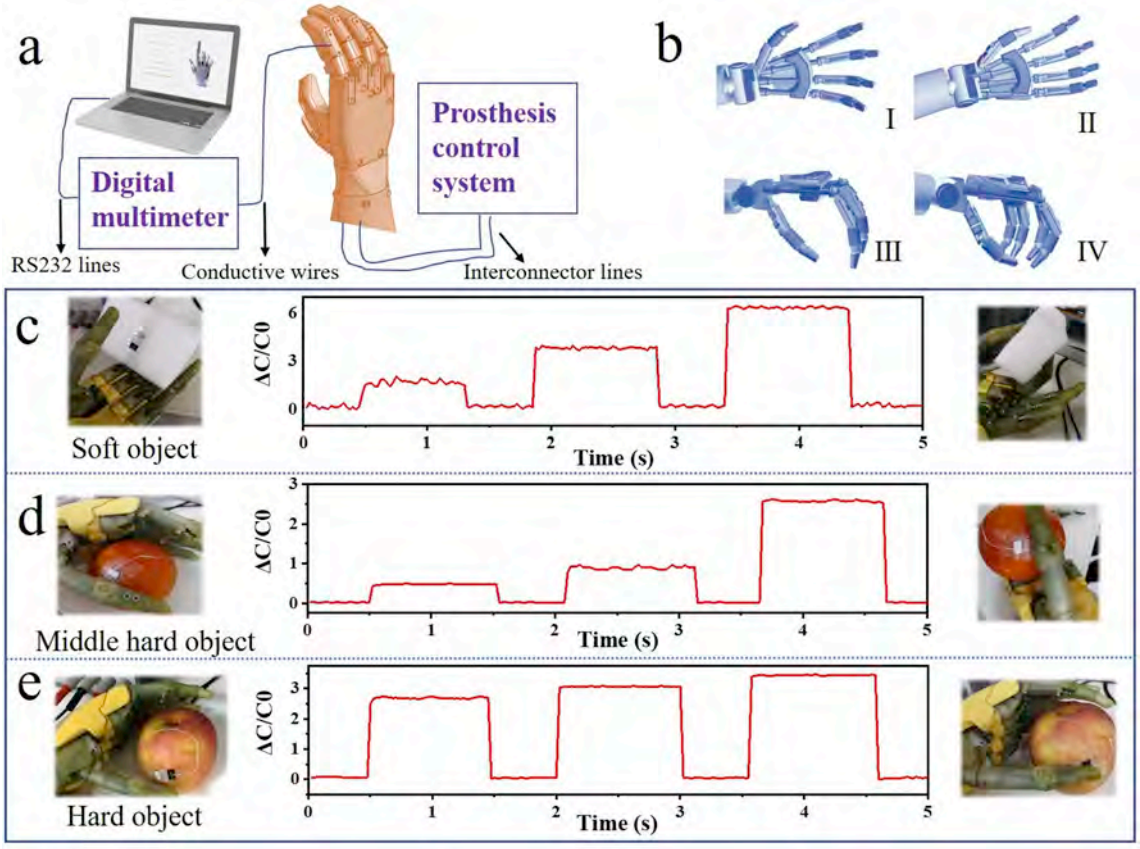

Fig. 7. Real-time monitoring of robotic hand grabbing objects. a) Schematic diagram of signal recording for robotic grabbing objects. b) Four representative gestures during the robot hand grabbing objects. c-e) The electrical signals monitored by the sensor attached on the objects with different hardness of sponge, tomato, and apple grabbed by robot hand, respectively.

screen of computer through LabVIEW. Fig. 7b illustrates four representative gestures of the robot hand from full relaxation (I) to tightly grasp (IV) during grabbing objects. Fig. 7c–e exhibit the electrical signal curves recorded from grabbing a sponge (soft object), a tomato (middle hard object) and an apple (hard object), respectively. The grabbing motions were carried out as relaxing ~0.5 s followed by holding ~1 s with three repeated cycles. It can be clearly observed that the up-hill and down-hill of curve represented the bending and opening state of the palm during the gripping process, and different heights of up-hill represented the magnitude of robot arm's force during gripping process (Movie S3, Supporting Information). For example, the sponge had the characteristics of light weight and easy deformation, so the received force by the robot was gradually increased during the process of being grasped. However, the apple was not only heavy but also the surface was not easily deformed, so that the signal of the sensor was always in a high state during the grip by the robot arm. In a word, outstanding experimental results illustrate that the capacitive sensor provides a facile, low-cost and highly-effective method to manage medical diagnosis and promote the human-machine interaction owing to its high-sensitivity, fast response behavior and excellent cyclic stability.

Supplementary data related to this article can be found at https://doi.org/10.1016/j.nanoen.2019.104436.

4. Conclusion

In summary, we have fabricated a flexible capacitive pressure sensor with ultrahigh sensitivity based on convex microarrays and ultrathin dielectric layer by a facile and low-cost strategy. The sensor demonstrates ultrahigh sensitivity of 30.2 kPa^{-1} (<130Pa), low limit of detection of 0.7 Pa, fast response time of 25 ms and outstanding stability upon 100 000 cycles. The FEA results reveal the microarrays on the electrode surface and ultrathin dielectric layer synergistically cause significant increase in contact area as well as huge reduce in distance between two electrodes when external pressure was applied on the sensor, ultimately resulting in high sensitivity. The flexible sensor has been successfully applied in monitoring various human biological signals and robot hand's motion, paving a way for the applications in smart health care, automatic speech recognition (ASR) and language recognition, and is expected to enter the big date era.

Declaration of competing interest

The authors declare that they have no known competing financial interests or personal relationships that could have appeared to influence the work reported in this paper.

Acknowledgements

The authors are grateful for the financial support from National Natural Science Foundation of China (61701488 and 21571186), National Key R&D Project from Minister of Science and Technology China (2016YFA0202702), Shenzhen Basic Research Plan (JCYJ20170818162548196), Shenzhen International Cooperation Project (GJHZ20180420180909654), National and Local Joint Engineering Laboratory of Advanced Electronic Packaging Materials (2017-934), Leading Scientific Research Project of Chinese Academy of Sciences (QYZDY-SSW-JSC010), SIAT CAS-CUHK Joint Laboratory of Materials and Devices for High Density Electronic Packaging, and Youth Innovation Promotion Association of the Chinese Academy of Sciences (2017411).

Appendix A. Supplementary data

Supplementary data to this article can be found online at https://doi.org/10.1016/j.nanoen.2019.104436.

References

[1] C. Pang, J.H. Koo, A. Nguyen, J.M. Caves, M.G. Kim, A. Chortos, K. Kim, P.J. Wang, J.B.H. Tok, Z.A. Bao, Adv. Mater. 27 (2015) 634–640.
[2] Y. Choi, E.C. Brown, S.M. Haile, W. Jung, Nano Energy 23 (2016) 161–171.
[3] T. Roberts, J.B. De Graaf, C. Nicol, T. Hervé, M. Fiocchi, S. Sanaur, Adv. Healthc. Mater. 5 (2016) 1462–1470.
[4] Q.J. Sun, X.H. Zhao, Y. Zhou, C.C. Yeung, W. Wu, S. Venkatesh, Z.X. Xu, J.J. Wylie, W.J. Li, V.A.L. Roy, Adv. Funct. Mater. 29 (2019) 1808829.
[5] L. Dhakar, P. Pitchappa, F.E.H. Tay, C. Lee, Nano Energy 19 (2016) 532–540.
[6] K.L. Xia, C.Y. Wang, M.Q. Jian, Q. Wang, Y.Y. Zhang, Nano Res. 11 (2018) 1124–1134.
[7] Z. Wang, L. Zhang, J. Liu, H. Jiang, C. Li, Nanoscale 10 (2018) 10691–10698.
[8] J.D. Shi, L. Wang, Z.H. Dai, L.Y. Zhao, M.D. Du, H.B. Li, Y. Fang, Small 14 (2018) 1800819.
[9] J. Park, J. Kim, J. Hong, H. Lee, Y. Lee, S. Cho, S.-W. Kim, J.J. Kim, S.Y. Kim, H. Ko, NPG Asia Mater. 10 (2018) 163–176.
[10] Y. Lee, J. Park, S. Cho, Y.E. Shin, H. Lee, J. Kim, J. Myoung, S. Cho, S. Kang, C. Baig, H. Ko, ACS Nano 12 (2018) 4045–4054.
[11] Y. Zhang, Y.G. Hu, P.L. Zhu, F. Han, Y. Zhu, R. Sun, C.P. Wong, ACS Appl. Mater. Interfaces 9 (2017) 35968–35976.
[12] X.T. Shuai, P.L. Zhu, W.J. Zeng, Y.G. Hu, X.W. Liang, Y. Zhang, R. Sun, C.P. Wong, ACS Appl. Mater. Interfaces 9 (2017) 26314–26324.
[13] Z. Lou, S. Chen, L.L. Wang, R.L. Shi, L. Li, K. Jiang, D. Chen, G.Z. Shen, Nano Energy 38 (2017) 28–35.
[14] C.F. Yang, L.L. Li, J.X. Zhao, J.J. Wang, J.X. Xie, Y.P. Cao, M.Q. Xue, C.H. Lu, ACS Appl. Mater. Interfaces 10 (2018) 25811–25818.
[15] K.Y. Lee, M.K. Gupta, S.-W. Kim, Nano Energy 14 (2015) 139–160.
[16] T.Q. Trung, N.E. Lee, Adv. Mater. 28 (2016) 4338–4372.
[17] H. Ghayvat, S. Mukhopadhyay, X. Gui, N. Suryadevara, Sensors 15 (2015) 10350–10379.
[18] X. Han, X. Chen, X. Tang, Y.L. Chen, J.H. Liu, Q.D. Shen, Adv. Funct. Mater. 26 (2016) 3640–3648.
[19] Q. Wang, M. Jian, C. Wang, Y. Zhang, Adv. Funct. Mater. 27 (2017) 1605657.
[20] S. Peng, P. Blanloeuil, S. Wu, C.H. Wang, Adv. Mater. Interfaces 5 (2018) 1800403.
[21] H. Kim, S.W. Lee, H. Joh, M. Seong, W.S. Lee, M.S. Kang, J.B. Pyo, S.J. Oh, ACS Appl. Mater. Interfaces 10 (2018) 1389–1398.
[22] Z. He, W. Chen, B. Liang, C. Liu, L. Yang, D. Lu, Z. Mo, H. Zhu, Z. Tang, X. Gui, ACS Appl. Mater. Interfaces 10 (2018) 12816–12823.
[23] S.H. Cho, S.W. Lee, S. Yu, H. Kim, S. Chang, D. Kang, I. Hwang, H.S. Kang, B. Jeong, E.H. Kim, S.M. Cho, K.L. Kim, H. Lee, W. Shim, C. Park, ACS Appl. Mater. Interfaces 9 (2017) 10128–10135.
[24] T. Li, H. Luo, L. Qin, X. Wang, Z. Xiong, H. Ding, Y. Gu, Z. Liu, T. Zhang, Small 12 (2016) 5042–5048.
[25] B.-Y. Lee, J. Kim, H. Kim, C. Kim, S.-D. Lee, Sens. Actuators A Phys. 240 (2016) 103–109.
[26] Y. Joo, J. Byun, N. Seong, J. Ha, H. Kim, S. Kim, T. Kim, H. Im, D. Kim, Y. Hong, Nanoscale 7 (2015) 6208–6215.
[27] G. Schwartz, B.C.K. Tee, J. Mei, A.L. Appleton, D.H. Kim, H. Wang, Z. Bao, Nat. Commun. 4 (2013) 1602790.
[28] X. Wang, Z. Liu, T. Zhang, Small 13 (2017) 1602790.
[29] C. Dagdeviren, P. Joe, O.L. Tuzman, K.-I. Park, K.J. Lee, Y. Shi, Y. Huang, J. A. Rogers, Extrem. Mech. Lett. 9 (2016) 269–281.
[30] J. Park, M. Kim, Y. Lee, H.S. Lee, H. Ko, Sci. Adv. 1 (2015) 1500661.
[31] S.K. Mahadeva, K. Walus, B. Stoeber, ACS Appl. Mater. Interfaces 7 (2015) 8345–8362.
[32] S. Xu, Y.-w. Yeh, G. Poirier, M.C. McAlpine, R.A. Register, N. Yao, Nano Lett. 13 (2013) 2393–2398.
[33] X. Wang, H. Zhang, L. Dong, X. Han, W. Du, J. Zhai, C. Pan, Z.L. Wang, Adv. Mater. 28 (2016) 2896–2903.
[34] X. Fan, J. Chen, J. Yang, P. Bai, Z. Li, Z.L. Wang, ACS Nano 9 (2015) 4236–4243.
[35] B. Meng, W. Tang, Z.-h. Too, X. Zhang, M. Han, W. Liu, H. Zhang, Energy Environ. Sci. 6 (2013) 3235–3240.
[36] P. Bai, G. Zhu, Z.-H. Lin, Q. Jing, J. Chen, G. Zhang, J. Ma, Z.L. Wang, ACS Nano 7 (2013) 3713–3719.
[37] F.-R. Fan, L. Lin, G. Zhu, W. Wu, R. Zhang, Z.L. Wang, Nano Lett. 12 (2012) 3109–3114.
[38] C. Pang, G.-Y. Lee, T.-i. Kim, S.M. Kim, H.N. Kim, S.-H. Ahn, K.-Y. Suh, Nat. Mater. 11 (2012) 795–801.
[39] J. Wang, J.T. Jiu, M. Nogi, T. Sugahara, S. Nagao, H. Koga, P. He, K. Suganuma, Nanoscale 7 (2015) 2926–2932.
[40] C.L. Choong, M.B. Shim, B.S. Lee, S. Jeon, D.S. Ko, T.H. Kang, J. Bae, S.H. Lee, K. E. Byun, J. Im, Y.J. Jeong, C.E. Park, J.J. Park, U.I. Chung, Adv. Mater. 26 (2014) 3451–3458.
[41] B.W. Zhu, Z.Q. Niu, H. Wang, W.R. Leow, H. Wang, Y.G. Li, L.Y. Zheng, J. Wei, F. W. Huo, X.D. Chen, Small 10 (2014) 3625–3631.
[42] J. Park, Y. Lee, J. Hong, M. Ha, Y.-D. Jung, H. Lim, S.Y. Kim, H. Ko, ACS Nano 8 (2014) 4689–4697.
[43] D. Kwon, T.-I. Lee, J. Shim, S. Ryu, M.S. Kim, S. Kim, T.-S. Kim, I. Park, ACS Appl. Mater. Interfaces 8 (2016) 16922–16931.
[44] Y. Wan, Z. Qiu, J. Huang, J. Yang, Q. Wang, P. Lu, J. Yang, J. Zhang, S. Huang, Z. Wu, C.F. Guo, Small 14 (2018) 1801657.
[45] Y. Hu, T. Zhao, P. Zhu, X. Liang, R. Sun, C.-P. Wong, RSC Adv. 5 (2015) 58–67.

Yaoxu Xiong is currently a M.S. student at Shenzhen Institutes of Advanced Technology, Chinese Academy of Sciences. He received his B.S. degree in Applied Chemistry at Yangtze University of in 2017. His recent research interest focuses on flexible electronic materials and devices.

Youkang Shen is a M.S. student at Shenzhen University, major in Materials Engineering, and now is studying at Shenzhen Institutes of Advanced Technology, Chinese Academy of Sciences. He received his B.S. degree from Jiangsu University of Science and Technology in 2018. His research interests focus on wearable electronics and electromagnetic interference (EMI) shielding nanocomposites.

Lan Tian received her M.S. degree in Biomedical Engineering from Southeast University in 2010. Since 2010, she has been with Shenzhen Institutes of Advanced Technology, Chinese Academy of Sciences. She is currently pursuing the Ph.D. degree in Pattern Recognition and Intelligent System in University of Chinese Academy of Sciences. Her current research interests include physiological signals acquisition, motion classification and prosthesis control.

Associate Prof. Yougen Hu received his B.S. and M.S. degrees in Polymer Materials and Engineering (2007) and Material Science (2010) from Jiangsu University, respectively, and obtained his Ph. D. degree in Pattern Recognition and Intelligent Systems at University of Chinese Academy of Sciences (2017). He joined Shenzhen Institutes of Advanced Technology, Chinese Academy of Sciences in 2010 and was appointed as associate professor in 2018. His research interest includes advanced electronic packaging materials, flexible electronic materials and devices, multi-functional micro/nano-structured materials. So far, he has published more than 20 peer-reviewed papers and held more than 50 China patents of which 24 has been issued.

Prof. Pengli Zhu received the Ph.D. degree from Institute of Chemistry, Chinese Academy of Sciences, Beijing, China, in 2010 and then joined Shenzhen Institutes of Advanced Technology, Chinese Academy of Sciences. Until now, she has published nearly 130 academic papers and held 80 patents, of which 20 has been issued. Her research interests are focused on the flexible printed or wearable electronic devices, metal nanomaterials, conductive nanocomposites used in the electronic packaging.

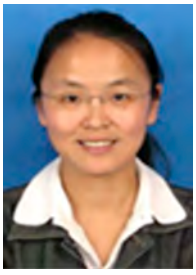

Prof. Rong Sun received her Ph.D. degree from Lanzhou Institute of Chemical Physics, Chinese Academy of Sciences, Lanzhou, China, in 2006. She currently is the director of the Center for Advanced Materials in Shenzhen Institutes of Advanced Technology, Chinese Academy of Sciences. She has devoted herself to research in the field of advanced electronic packaging since 2006. Dr. Sun has authored or co-authored more than 300 journal papers and held over 200 China patents. Her current research interests include Flip-Chip Underfill, Through Silicon Via (TSV), Thermal Interface Materials (TIM), Embedded Capacitor Inductor Resistance, Flexible Substrates, and the key inorganic nanomaterials.

Prof. C.P. Wong received the B.S. degree in chemistry from Purdue University, West Lafayette, IN, and the Ph.D. degree in chemistry from Pennsylvania State University, University Park, in 1975. After his doctoral study, he was awarded a postdoctoral fellowship under Nobel laureate Prof. Henry Taube at Stanford University. He joined AT&T Bell Laboratories, PA, in 1977 as Member of Technical Staff and became an AT&T Bell Laboratories Fellow in 1992. Dr. Wong currently is the Charles Smithgall Institute Endowed Chair and Regents' Professor at Georgia Institute of Technology (Georgia Tech), Atlanta. His research interests lie in the fields of polymeric electronic materials, electronic, photonic and MEMS packaging and interconnect, interfacial adhesions, and nano-functional material syntheses and characterizations. He holds over 50 U S. patents, numerous international patents, has published over 1000 technical papers, 10 books and a member of the National Academy of Engineering of the USA since 2000.